Earthquakes and Structures, *Vol. 9, No. 5 (2015) 1115-1132*
DOI: http://dx.doi.org/10.12989/eas.2015.9.5.1115

Optimal input cross-power spectra in shake table testing of asymmetric structures

S. Ammanagi[1,2a] and C.S. Manohar[*1]

[1]Department of Civil Engineering, Indian Institute of Science, Bangalore 560 012, India
[2]Bangalore Integrated System Solutions (P) Ltd., Bangalore 560058, India

(Received February 15, 2015, Revised July 21, 2015, Accepted July 23, 2015)

Abstract. The study considers earthquake shake table testing of bending-torsion coupled structures under multi-component stationary random earthquake excitations. An experimental procedure to arrive at the optimal excitation cross-power spectral density (psd) functions which maximize/minimize the steady state variance of a chosen response variable is proposed. These optimal functions are shown to be derivable in terms of a set of system frequency response functions which could be measured experimentally without necessitating an idealized mathematical model to be postulated for the structure under study. The relationship between these optimized cross-psd functions to the most favourable/least favourable angle of incidence of seismic waves on the structure is noted. The optimal functions are also shown to be system dependent, mathematically the sharpest, and correspond to neither fully correlated motions nor independent motions. The proposed experimental procedure is demonstrated through shake table studies on two laboratory scale building frame models.

Keywords: random vibration; multi-component earthquake support motion; critical excitation models; shake table testing

1. Introduction

In dealing with dynamic response of bending-torsion coupled asymmetric structures under multi-component earthquake support motions, the correlations that exist between the excitation components is expected to play a crucial role. The idea of principal direction for excitation components along which the components are instantaneously uncorrelated is well-known (see, Kubo and Penzien 1979 for early studies and Rezaeian and Kiureghian 2012 for a more recent perspective). The principal axes of excitation, most often, do not coincide with the principal axes of the structure, thereby, leading to coupled bending-torsion oscillations of the structure. The mismatch of excitation and structural principal axes is clearly associated with the angle of incidence of seismic waves on the structure. The problem of estimating the least favourable angle of incidence for a given structure has been tackled by a few authors (see, for example, Singh and Ashtiany 1984, Lopez and Torres 1997). The development of modal combination rules taking into

∗Corresponding author, Professor, E-mail: manohar@civil.iisc.ernet.in
[a]Research Student, E-mail: somayya@civil.iisc.ernet.in

http://www.techno-press.org/journals/eas&subpage=7 ISSN: 2092-7614 (Print), 2092-7622 (Online)

account issues related to angle of incidence in response spectrum based response analysis has also been tackled **(**see, for example, Kiureghian and Nakamura 1993, Menun and Kiureghian 1998, 2000, Lopez *et al*. 2000, Gonzalez *et al*. 2015). The study by Athanatopoulou (2005) proposes an analytical procedure to determine the critical angle of incidence in terms of response of the structure to two specific loading cases. The study shows that the critical angle of incidence can produce response which is about 80% higher than the response for the case when the excitation and structural principal axes coincide. The review paper by Reyes-Salazar *et al*. (2008) provide detailed review of issues connected with structural response to mufti-component seismic support motions specifically with reference to prevailing codified design procedures. The importance of including the effect of seismic angle of incidence in evaluating seismic fragility of bridge structures has been pointed out by Torbol and Shinozuka (2012). In the context of seismic qualification testing of nuclear power plant equipment under multi-component earthquake support motions, there exist guidelines on including the effect of directionality in load specifications (IEEE-344 2013) with emphasis on ensuring conservative estimates of the response.

A random vibration analysis based approach to determine the optimal cross-psd functions between excitation components which lead to highest or lowest response variance has been developed by Sarkar and Manohar (1996, 1998**).** Specifically these authors have demonstrated the existence of excitation cross-psd function models which correspond neither to fully correlated motions nor to independent motions and have outlined analytical procedures to arrive at these optimal cross-psd functions in terms of frequency response functions. Abbas and Manohar (2007) have considered parametrically excited structures under combined vertical and horizontal earthquake support motions and determined the optimal seismic excitation psd models which minimize time variant reliability defined respect to a specified response process. These studies belong to the broader class of load modelling approaches which could be classified as critical excitation modelling. Extensive accounts of development of critical excitation modelling in earthquake engineering, including issues related to multi-component earthquake load modelling, have been provided by Takewaki (2002, 2013).

The present study considers the problem of experimental determination of the optimal cross-psd function models in the study of earthquake response of structures subjected to multi-component earthquake ground motions. It is demonstrated that the procedure developed by Sarkar and Manohar (1996, 1998) can be generalized to achieve this. This idea is demonstrated by conducting earthquake shake table studies on two building frame models. The building frame models are designed to display bending-torsion coupling and shake table used is capable of applying multi-axis ground motion. The study assumes the earthquake excitation components are modelled as jointly stationary zero-mean Gaussian random processes. Furthermore, the auto-psd functions of the excitation components are taken to be specified while the cross-psd functions are not. These unknown cross-psd functions are determined so that the steady state variance of a chosen response variable is maximized/minimized and this exercise is shown to be based on solely an experimental procedure which bypasses the need for developing an idealized mathematical model for the structure under study. The bounds on the response quantity thus obtained are demonstrated to be mathematically the sharpest in nature. We would like to note that issues related optimal cross-psd function models in the context of spatially varying support motions has been recently addressed in a separate study, albeit in a different context (namely, that of vibration testing of a four-wheeled vehicle on a four-post test rig for road roughness induced oscillations), by present authors (Ammanagi and Manohar 2015).

2. Basis for the experimental procedure

Consider a linear time invariant structural system acted upon by multi-component support accelerations. It is assumed that the extent of the structure is such that the spatial variability in ground motions can be neglected. By assuming that the system starts from rest, any generic response $Y(t)$ of the structure (for example, one of the displacement, strain, or stress components) can, in principle, be written as

$$Y(t) = \int_0^t \sum_{i=1}^{3} h_i(t-\tau) X_i(\tau) d\tau \tag{1}$$

Here $X_i(t), i=1,2,3$ are the three support motion components, and $h_i(t)$ is the impulse response function which relates the excitation component $X_i(t)$ to the response $Y(t)$. The functions $h_i(t); i=1,2,3$, can either be derived based on a postulated finite element model for the structure system, or, based on direct measurements in a laboratory. We focus in the present study on the latter option and take that the structure under study already exists and is being tested on a shake table. It may be noted that the techniques for measuring the impulse response functions, or, equivalently, the frequency response functions, are well established in the existing literature (Ewins 2000, McConnel 1995, Bendat and Piersol 2010). Thus, by measuring $h_i(t); i=1,2,3$, experimentally, we are eliminating the need to introduce idealizations associated with complicating issues, such as, modelling constitutive relations, damping model, joint flexibility, and boundary conditions, which otherwise would be inevitable if one were to arrive at these functions via computational modelling. We model $X_i(t), i=1,2,3$ as a set of stationary, zero mean, Gaussian random processes with the associated power spectral density (psd) function matrix $S(\omega)=[S_{ij}(\omega)]; i,j=1,2,3$. In the steady state, the response psd function can be obtained as

$$S_{YY}(\omega) = \sum_{i,j=1,3} H_i(\omega) S_{ij}(\omega) H_j^*(\omega) \tag{2}$$

Here $H_i(\omega)$ is the complex frequency response function being the Fourier transform of the impulse response function $h_i(t)$, and a * represents complex conjugation. By noting that $S_{ij}(\omega) = \sqrt{S_{ii}(\omega) S_{jj}(\omega)} \exp\left[-\mathrm{i}\theta_{ij}(\omega)\right]$, the response variance can be written as

$$\sigma_{YY}^2 = \int_{-\infty}^{\infty} \sum_{i=1,3} \left|H_i(\omega)\right|^2 S_{ii}(\omega) d\omega + \int_{-\infty}^{\infty} \sum_{\substack{i,j=1,3 \\ i \neq j}} H_i(\omega) S_{ij}(\omega) H_j^*(\omega) d\omega \tag{3}$$

Now we consider the situation in which the input is partially specified such that the auto-psd functions $S_{ii}(\omega); i=1,2,3$, are taken to be given while the cross-psd functions $S_{ij}(\omega)$ $i \neq j=1,2,3$ are not known. We aim to determine the bounds on these unknown functions which produce the lowest and highest steady state response variances denoted respectively by $\underline{\sigma}_{YY}^2$ and $\bar{\sigma}_{YY}^2$. This situation would be similar to the case in which the excitations are specified along their principal directions and one would be interested in knowing the optimal angles of incidence which maximize/minimize a chosen response variable. While solving this optimization problem, it should be noted that the unknown cross-psd functions satisfy the constraints

$$\begin{aligned} &0 \le \left|S_{ij}(\omega)\right| \le \sqrt{S_{ii}(\omega) S_{jj}(\omega)}; \\ &S_{ji}(\omega) = S_{ij}^*(\omega)\, i \neq j = 1,2,3 \end{aligned} \tag{4}$$

The first of these constraints follows from the application of the Schwarz inequality on the definition of the cross-psd function (Papoulis and Pillai 2002; section 9.3, equations 9.179-9.181). The above stated constrained optimization problem can be handled analytically (using, for example, the calculus of variations), numerically, or, more simply by direct inspection (Sarkar and Manohar 1996, 1998). To see this, we note that $S_{ji}(\omega)=S_{ij}^*(\omega)$ and obtain $H_i(\omega)H_j^*(\omega)S_{ij}(\omega)+H_j(\omega)H_i^*(\omega)S_{ji}(\omega)=2\,\mathrm{Re}\left[H_i(\omega)H_j^*(\omega)S_{ij}(\omega)\right]$. Furthermore, by writing $\tilde{H}_{ij}(\omega)=H_i(\omega)H_j^*(\omega)=\left|\tilde{H}_{ij}(\omega)\right|\exp\left[\mathrm{i}\theta_{ij}(\omega)\right]$ and $S_{ij}(\omega)=\left|S_{ij}(\omega)\right|\exp\left[-\mathrm{i}\phi_{ij}(\omega)\right]$, we get

$$H_i(\omega)H_j^*(\omega)S_{ij}(\omega)+H_j(\omega)H_i^*(\omega)S_{ji}(\omega)=2\left|\tilde{H}_{ij}(\omega)\right|\left|S_{ij}(\omega)\right|\cos\left[\theta_{ij}(\omega)-\phi_{ij}(\omega)\right] \quad (5)$$

To proceed further, we introduce further notations

$$\begin{aligned}
&\left|\tilde{H}_{ij}(\omega)\right|=\sqrt{G_{1,ij}^2(\omega)+G_{2,ij}^2(\omega)};\theta_{ij}(\omega)=\tan^{-1}\left[\frac{G_{2,ij}(\omega)}{G_{1,ij}(\omega)}\right]\\
&G_{1,ij}(\omega)=\mathrm{Re}\left[H_i(\omega)\right]\mathrm{Re}\left[H_j(\omega)\right]+\mathrm{Im}\left[H_i(\omega)\right]\mathrm{Im}\left[H_j(\omega)\right]\\
&G_{2,ij}(\omega)=\mathrm{Im}\left[H_i(\omega)\right]\mathrm{Re}\left[H_j(\omega)\right]-\mathrm{Im}\left[H_j(\omega)\right]\mathrm{Re}\left[H_i(\omega)\right]\\
&i,\ j=1,\ldots 3,\ \ j>i
\end{aligned} \quad (6)$$

In order to determine the bounds $\underline{\sigma}_{YY}^2$ and $\overline{\sigma}_{YY}^2$, we note that the contributions from the first term in Eq. (3) are always positive while the second set of terms could make positive or negative contributions. If few we select

$$\left|S_{ij}(\omega)\right|=\sqrt{S_{ii}(\omega)S_{jj}(\omega)} \text{ and } \phi_{ij}(\omega)=\theta_{ij}(\omega),\quad \forall\ \omega\geq 0 \quad (7)$$

it can be deduced that the contribution from the second set of terms would be always positive and hence the resulting response would lead to the upper bound $\overline{\sigma}_{YY}^2$. Conversely, if we select

$$\left|S_{ij}(\omega)\right|=\sqrt{S_{ii}(\omega)S_{jj}(\omega)} \text{ and } \phi_{ij}(\omega)=\theta_{ij}(\omega)+\pi,\quad \forall\ \omega\geq 0 \quad (8)$$

the contributions from the second set of terms would always be negative, thereby leading to the lower bound response $\underline{\sigma}_{YY}^2$. Thus, the models in Eqs. (7) and (8), provide the desired optimal models for the cross-psd functions which, in turn, provide, respectively, the upper and lower bounds on the response variance σ_Y^2.

Remarks

(a) The optimal cross-psd models are system and response variable dependent and correspond neither to the case of excitation components being fully correlated nor the components being independent.

(b) The bounds $\underline{\sigma}_{YY}^2$ and $\overline{\sigma}_{YY}^2$ on the response thus obtained are mathematically the sharpest in nature. This is because the constraints stated in Eq. (4) are exactly satisfied and no approximations have been made in arriving at bounds $\underline{\sigma}_{YY}^2$ and $\bar{\sigma}_{YY}^2$.

(c) The determination of the phase spectra $\theta_{ij}(\omega)$; $i\neq j$=1,2,3, hold the key to the determination of the optimal input and response models. These spectra could be determined experimentally in terms of the measured FRFs, $H_i(\omega);i$=1,2,3.

(d) While the earlier study by Sarkar and Manohar (1996, 1998) focussed on analytical determination of the optimal load and response models, we consider in this study the problem of determining these functions experimentally. It is believed that this approach provides a counter point to the presently existing guidelines on testing structures under multi-component excitations in which the issue of angle of incidence of seismic wave is considered in an empirical manner (IEEE-344 2013). It is emphasised that the methods for measuring FRF-s are well established in the literature (Ewins 2000, McConnel 1995, Bendat and Piersol 2010) and the novel element of the present study lies in identifying specific forms of FRF-s which can be processed further to determine the optimal input cross-psd models which lead to the highest and lowest responses.

3. Experimental procedure

We consider the problem of seismic qualification testing of a given structure for a specified multi-component earthquake excitation using a multi-axes shake table. The load specification is taken to be in terms of the auto-psd functions $S_{ii}(\omega);i$=1,2,3 of the components of support motion with the cross-psd functions $S_{ij}(\omega)$ $i\neq j$=1,2,3 being not known. One can conceive such situation when the earthquake loads are specified in terms of a set of smooth design response spectra along the three axes and one could deduce a corresponding set of compatible auto-psd functions for each of the components (Nigam and Narayanan 1994). In such an exercise, the cross-psd functions would essentially remain unspecified. The structure under study is taken to be characterized by coupling between bending in two directions and torsion (see Figs.1 and 2 and Annexure A for details of structures which are considered in this study). The cross-psd functions play a crucial role in deciding upon the worst (and the most favourable) combination of excitation axes (reflecting the angle of incidence of the seismic wave) and the principal axes of the structure. The steps for an experimental procedure, based on the formulation presented in the preceding section, to determine the optimal cross-psd functions $S_{ij}(\omega)$ $i\neq j$=1,2,3 and the response bounds $\underline{\sigma}_{YY}^2$ and $\bar{\sigma}_{YY}^2$, are as follows:

Step-1 For a specified response variable, measure the frequency response functions $H_i(\omega);i$=1,2,3. This is done by using single-input single-output method where a band limited white noise excitation is applied along one of the axes and the desired response time history is measured. The sample realization of the FRF $H_i(\omega)$ is obtained by using the relation $H_i(\omega)=\dfrac{P_{XY}(\omega)}{P_{XX}(\omega)}$ where $P_{XY}(\omega)$ is cross-psd between input and the output and $P_{XX}(\omega)$ is auto-psd of the input. Subsequently, an estimator for $H_i(\omega)$ is obtained by averaging these realizations over an ensemble of N_s realizations. In the numerical work to follow, we take N_s=1000.

Step-2 Estimate the optimal cross-psd functions $S_{ij}(\omega)$ $i\neq j$=1,2,3 using Eqs. (7) and (8).

Step-3 Evaluate the response bounds $\underline{\sigma}_{YY}^2$ and $\bar{\sigma}_{YY}^2$ using Eqs. (2) and (3).

Step-4 Simulate an ensemble of $X_i(t),i$=1,2,3 compatible with the given auto-psd functions $S_{ii}(\omega)$;i=1,2,3 and the optimal cross-psd functions determined in steps 1 and 2 above. This can be done by using the well-known procedure based on Fourier representation of sample time histories (Nigam and Naryanan 1994). Test the structure for this ensemble of excitations and estimate the response psd function based on the measured ensemble of response time histories. Subsequently, compute the associated response variances by evaluating the area under the computed psd function.

Remarks

(a) The response bounds $\underline{\sigma}_{YY}^2$ and $\bar{\sigma}_{YY}^2$ can be evaluated using Eqs. (2) and (3) once the optimal cross-psd functions are obtained in step 2 and one need not proceed to step 4. This, however, may not be consistent with the objectives of earthquake qualification testing which intends to test the structure under earthquake like loads.

(b) To gain confidence in the correctness of the results obtained, additional tests could optionally be done with $X_i(t), i=1,2,3$ being fully correlated, or, independent, so that the corresponding estimates of the response psd functions and variances could be obtained for the purposes of comparison.

(c) Additionally, one could test the structure for a family of excitations given by $\tilde{X}(t) = T(\theta) X(t)$ for different values of θ, where $T(\theta)$ is a rotation matrix and θ is a parameter characterizing the angle of incidence of the seismic wave. The results on maximum and minimum response variances, thus obtained, would provide a means to assess the results obtained based on optimal cross-psd model developed in the preceding sections.

(d) The method, as developed, is applicable only to linear time invariant systems. Extensions to include possible nonlinear behaviour is indeed of interest in earthquake engineering especially since one of the objectives of earthquake resistant design is to achieve controlled inelastic behaviour and codes of practice allow for inelastic responses under design basis and maximum credible earthquakes (see, for example, the discussion by Jaiswal and Sinha 2007 in the context of Indian codes of practice). Moreover, the framework of performance based earthquake engineering also requires the ability to handle nonlinear behaviour since questions on structural performance at increasingly severe excitation levels need to be addressed. Within the framework of computational studies one could obtain approximate solutions for the optimal cross-psd functions via the method of equivalent linearization, or, more acceptable solutions, through Monte Carlo simulations and numerical optimization schemes. However, there is no obvious way of extending such approaches to tackle the problem through purely experimental procedures. One possible alternative is to adopt the Volterra-Wiener expansion for the nonlinear system response (see, for example, Bendat 1998, Worden and Tomlinson 2001) and re-write Eq. (1) as

$$Y(t) = \int_0^t \sum_{i=1}^{3} h_i^I(t-\tau) X_i(\tau) d\tau + \sum_{i=1}^{3}\sum_{j=1}^{3}\int_0^t\int_0^t h_{ij}^{II}(t-\tau_1, t-\tau_2) X_i(\tau_1) X_i(\tau_2) d\tau_1 d\tau_2 + \cdots \quad (9)$$

where $h_i^I(t), h_{ij}^{II}(t_1,t_2), \cdots$ are respectively the first, second, and higher order impulse response functions. For the purpose of illustration, the above series is truncated at the second term, and, by using the Fourier transform techniques, it can be shown that

$$
\begin{aligned}
S_{YY}(\omega) &= \sum_{i=1}^{3}\sum_{j=1}^{3} H_i^I(\omega) S_{ij}(\omega) H_i^{I*}(\omega) \\
&+ \sum_{i=1}^{3}\sum_{j=1}^{3}\sum_{i'=1}^{3}\sum_{j'=1}^{3} \frac{1}{2\pi}\int_{-\infty}^{\infty} H_{ij}^{II}(\omega_1,\omega-\omega_1) S_{ii'}(\omega_1) S_{jj'}(\omega-\omega_1) H_{i'j'}^{II*}(\omega_1,\omega-\omega_1)\, d\omega_1 + \\
&\sum_{i=1}^{3}\sum_{j=1}^{3}\sum_{i'=1}^{3}\sum_{j'=1}^{3} \frac{1}{2\pi}\int_{-\infty}^{\infty} H_{ij}^{II}(\omega_1,\omega-\omega_1) S_{ij'}(\omega_1) S_{ji'}(\omega-\omega_1) H_{ij}^{II*}(\omega_1,\omega-\omega_1)\, d\omega_1
\end{aligned}
\tag{10}
$$

which is the generalization of Eq. (2) for the case of nonlinear systems. Here $H_i^I(\omega)$ and $H_{ij}^{II}(\omega_1,\omega_2)$ are the first and the second order FRF-s which are, respectively, the one-dimensional and two-dimensional Fourier transforms of $h_i^I(t)$ and $h_{ij}^{II}(t_1,t_2)$. It may be noted that for a linear system $H_i^I(\omega) = H_i(\omega)$ and $H_{ij}^{II}(\omega_1,\omega_2) = 0$. The above equation can further be recast as

$$
\begin{aligned}
S_{YY}(\omega) &= \sum_{i=1}^{3}\left|H_i^I(\omega)\right|^2 S_{ii}(\omega) + \sum_{i=1}^{3}\sum_{j=1}^{3}\frac{1}{\pi}\int_{-\infty}^{\infty}\int_{-\infty}^{\infty}\left|H_{ij}^{II}(\omega_1,\omega-\omega_1)\right|^2 S_{ii}(\omega_1) S_{jj}(\omega-\omega_1)\, d\omega_1 \\
&+ \sum_{\substack{i,j\\ i\neq j}}^{3} H_i^I(\omega) S_{ij}(\omega) H_i^{I*}(\omega) + \sum_{\substack{i,i',j,j'\\ i\neq i',\, j\neq j'}}^{3} \frac{1}{2\pi}\int_{-\infty}^{\infty} H_{ij}^{II}(\omega_1,\omega-\omega_1) S_{ii'}(\omega_1) S_{jj'}(\omega-\omega_1) H_{i'j'}^{II*}(\omega_1,\omega-\omega_1)\, d\omega_1 \\
&+ \sum_{\substack{i,i',j,j'\\ i\neq j',\, j\neq i'}}^{3} \frac{1}{2\pi}\int_{-\infty}^{\infty} H_{ij}^{II}(\omega_1,\omega-\omega_1) S_{ij'}(\omega_1) S_{ji'}(\omega-\omega_1) H_{i'j'}^{II*}(\omega_1,\omega-\omega_1)\, d\omega_1
\end{aligned}
\tag{11}
$$

As has been done in interpreting Eq. (3), it can again be noted that the first two terms in the above equation always make positive contributions and last three the terms, involving the unknown cross-psd functions $S_{ij}(\omega)$, can again be determined to ensure that the sum of the contributions from these terms results in the highest positive contribution thereby leading to the upper bound on the response variance. Similar calculations can also be performed, so that the sum of the contributions from the last three terms results in the lowest negative contribution, leading to the lower response bound. While the determination of such bounds for linear systems has been straightforward (Eqs. (7)-(8)), for nonlinear systems, however, additional difficulties, arising due to presence of quadrature terms and products of cross-psd terms, need to be tackled. Also, in the experimental work, the establishment of response bounds would now require additional efforts in estimating the higher order FRF-s. Methods for achieving this indeed are available in the existing literature (Worden and Tomlinson 2001). In the present study we limit our attention to the treatment of only the linear systems and we propose to pursue extensions to nonlinear systems in a future study.

4. Illustrations

The procedure developed in the preceding sections is illustrated with the help of two simple steel frame models as shown in Figs. 1 and 2. The first of these models consists of a rigid slab supported by four inclined columns of differing lengths. The slab is attached with three additional plates to create asymmetry in mass distribution. This frame is taken to be acted upon by three-component earthquake support motions and, given the presence of inclined columns, the inclusion of vertical component of excitation is particularly relevant. Fig. 2 shows a three-storied building frame model which has an L-shape in plan. The frame has rigid steel slabs appended with three additional plates as shown. This frame is shown to be acted upon by bidirectional horizontal earthquake support motions. In both these frames, one could expect coupling between two bending and torsional oscillations. The two frames were designed so that the first three natural frequencies were respectively as follows: frame-I: 8.21, 10.46, 21.25 Hz; frame-II: 7.83, 7.86 and 10.92 Hz. In both the frames the first two modes predominantly were bending in the two horizontal directions and third predominantly torsional about the vertical axis. It is believed that the two frames chosen for the study contain several of the complicating features which one could expect in realistic systems which require to be tested for seismic performance. Beyond this consideration, these frame models do not actually represent any specific prototype systems. The auto-psd of the horizontal support accelerations were taken to be identical and of the form (Clough and Penzien 1993).

$$S(\omega) = S_0 \frac{\omega^4\left[\omega_s^4 + \left(2\eta_s\omega_s\omega\right)^2\right]}{\left[\left(\omega_s^2-\omega^2\right)^2 + 2\eta_s\omega_s\omega\right]\left[\left(\omega_f^2-\omega^2\right)^2 + 2\eta_f\omega_f\omega\right]} \tag{12}$$

with ω_s=30 rad/s, η_s=0.8, ω_f=2 rad/s, η_f=0.99, S_0=0.005 (m/s^2)^2/(rad/s). The auto-psd of the vertical component was taken to be 0.5$S(\omega)$. The frames were instrumented with tri-axial accelerometers, angular accelerometers and strain gauges, and, these details, along with the details of frame geometry, are provided in Annexure A. The shake table used in this study has the capability to apply six-component support motions (three translations and three rotations) using a set of eight servo hydraulic actuators, 1 m×1 m table size, payload capacity of 500 kg, and a power pack with 65 litre per minute capacity. The data acquisition system used has 96 channels with simultaneous sample and hold board, anti-aliasing filters, and permitted sampling rates up to 200 kS/s.

The frequency response functions $H_i(\omega)$, i=1,2,3 were measured using the samples of band limited white noise (0.05-25 Hz) by averaging across 1000 samples of 25 s duration. The response data were acquired at the rate of 200 samples/s. A bandpass filter with 0.05-50 Hz was used to mitigate the effect of noise. The estimation of the response psd (step-3) was carried out with 250 samples with the response time histories being sampled again at 200 samples/s. The response of the frames was studied for the following cases: (I) $X_i(t)$, i=1,2,3 are statistically independent, (II) the cross-psd functions of $X_i(t)$, i=1,2,3 are in-phase such that $S_{ij}(\omega)=\sqrt{S_{ii}(\omega)S_{jj}(\omega)}$, (III) the cross-psd functions of $X_i(t)$, i=1,2,3 are out-of-phase such that $S_{ij}(\omega)=-\sqrt{S_{ii}(\omega)S_{jj}(\omega)}$, (IV) the cross-psd functions of $X_i(t)$, i=1,2,3 correspond to the most favourable excitation model such that $S_{ij}(\omega)=\sqrt{S_{ii}(\omega)S_{jj}(\omega)}\exp\left[-\mathrm{i}\left(\phi_{ij}(\omega)+\pi\right)\right]$ and (V) the cross-psd functions of $X_i(t)$, i=1,2,3 correspond to the least favourable excitation model such that $S_{ij}(\omega)=\sqrt{S_{ii}(\omega)S_{jj}(\omega)}\exp\left[-\mathrm{i}\phi_{ij}(\omega)\right]$. Additionally, the system response with the support accelerations $Y_i(t)$, i=1,2,3 obtained using

$$\tilde{X}(t)=T(\theta)X(t);\quad T(\theta)=\begin{bmatrix}\cos\theta & \sin\theta & 0\\ -\sin\theta & \cos\theta & 0\\ 0 & 0 & 1\end{bmatrix} \tag{13}$$

for different values of $\theta=n\Delta\theta,\Delta\theta=10,i=0,1,2,\cdots,36$ were also considered. From this an estimate of the most favourable and the least favourable angle of incidence were obtained and these cases are designated, respectively, as VI and VII.

Tables 1 and 2, respectively, summarize the results on response standard deviations obtained for the frames I and II. The nomenclature for sensor labels is explained in Annexure A. For the purpose of detailed illustrations, response variables $a_1(t)$ (acceleration) of frame-I and $\varepsilon_{15,yy}(t)$ (bending strain) of frame-II are considered. Figs. 3 and 4, respectively, show measured frequency response functions of $a_1(t)$ and $\varepsilon_{15,yy}(t)$. The corresponding critical phase spectra determined by using Eqs. (7) and (8), for $a_1(t)$ and $\varepsilon_{15,yy}(t)$, are shown in Figs. 5 and 6 respectively. Figs. 7 and 8 show, respectively, spectra $G_{1,ij}(\omega)$ and $G_{2,ij}(\omega)$, determined using Eq. (6), associated with optimal phase spectra of $a_1(t)$ and $\varepsilon_{15,yy}(t)$. The auto-psd of $a_1(t)$ and $\varepsilon_{15,yy}(t)$ determined by using Eqs. (2) and (3) for loading cases I-V are shown in Figs. 9 and 10. Figs. 11 and 12 show, respectively, the variation of standard deviation of responses $a_1(t)$ and $\varepsilon_{15,yy}(t)$ as a function of angle of incidence. Here the most favourable and least favourable responses are also marked for sake of reference although it is understood that these optimal responses do not vary with respect to θ**.**

The response auto-psd functions depicted in Figs. 9 and 10 clearly show that the area under the spectra corresponding to the most favourable cross-psd model (case-IV) and the least favourable cross-psd model (case-V) provide, respectively, the lower and upper bounds on the response. Similarly, from Figs. 11 and 12 it is observed that the standard deviation obtained as a function of the angle of incidence lies within the lower and upper bounds of standard deviations determined

Fig. 1 An asymmetric frame with inclined columns under three-component support motions (Frame-I)

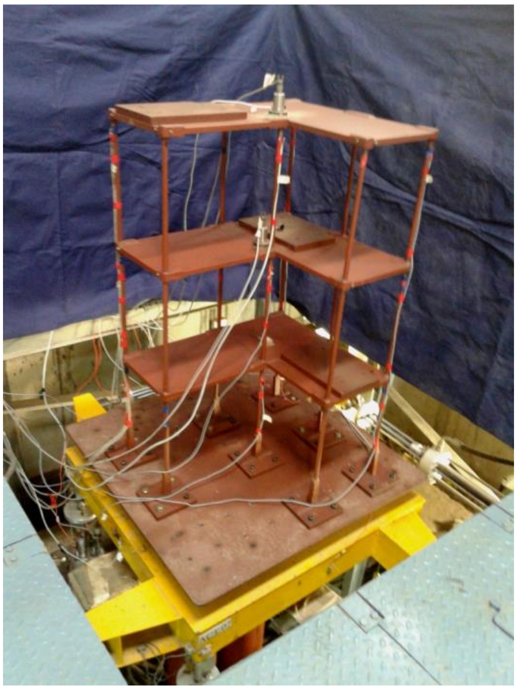

Fig. 2 An L-shaped frame under bi-directional horizontal support motions (Frame-II)

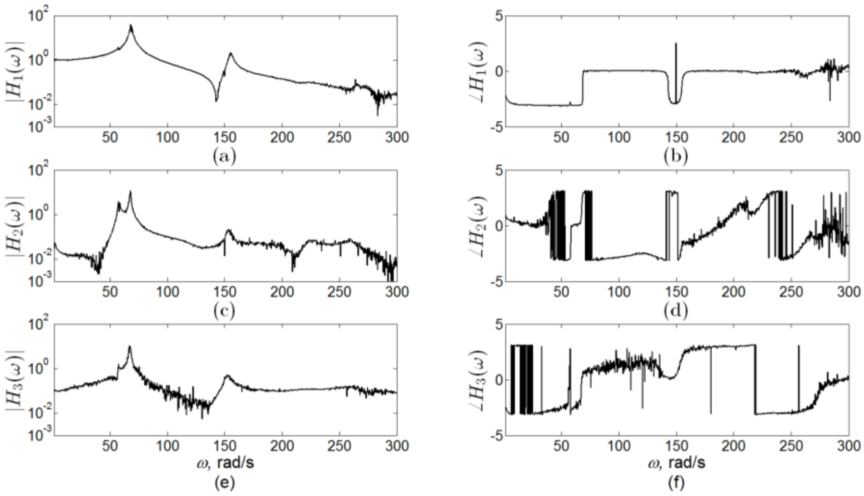

Fig. 3 FRFs $H_i(\omega)$;i=1,2,3 for $a_1(t)$ of frame-I; (a) $|H_1(\omega)|$; (b) $\angle H_1(\omega)$; (c) $|H_2(\omega)|$; (d) $\angle H_2(\omega)$; (e) $|H_3(\omega)|$; (f) $\angle H_3(\omega)$; note that $H_i(\omega)$;i=1,2,3 are non-dimensional

using critical phase spectra obtained using Eqs. (7) and (8). Likewise, the results presented in Tables 1 and 2 show that the response standard deviations obtained using excitations tailored to possess the optimal cross-psd models (cases IV and V) produce responses higher than those produced by other excitation models considered. Relatively minor exceptions to this occur in a few cases, namely, S.Nos. 3 and 8 in Table 1, and S.No. 13 in Table 2. Here it is observed that the response produced by case VII (that is, when the angle of incidence is varied over 0 to 360 degrees, see Eq. (13)) is slightly higher than the response produced by the critical cross-psd model (case V). While this difference is very minor for frame II (S.No.13 in Table 2), which could be attributed to sampling fluctuations and other experimental errors, the difference observed for frame I (S.Nos. 3 and 8 in Table 1) could additionally be due to the fact that in this case we are considering not only two horizontal earthquake excitation components, but also, a vertical component. The presence of vertical component, in principle, could make the system to become time varying in nature (due to interaction of forces due to vertical acceleration and self-weight to interact with horizontal displacements). While this effect gets accounted for in the determination of critical angle of incidence in cases VI and VII, their effect, however, are ignored while developing the optimal cross-psd models (cases IV and V) as the experimental procedure for developing these models assumes the system to be time-invariant in nature.

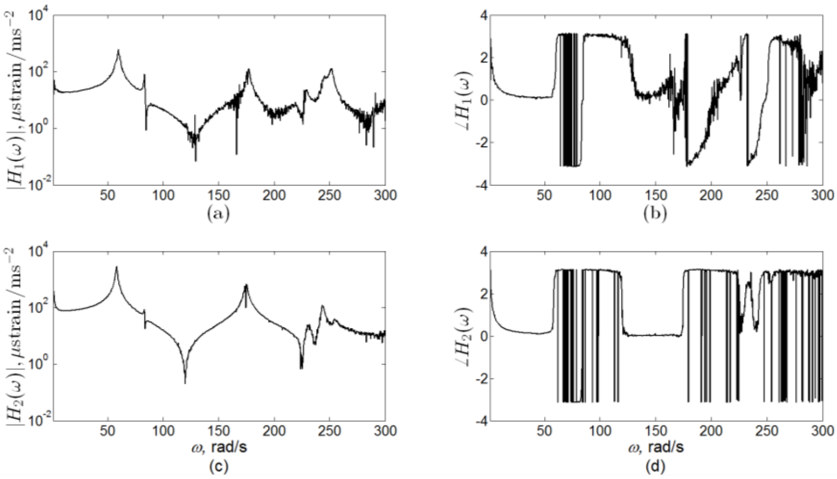

Fig. 4 FRFs $H_i(\omega)$;i=1,2 for $\varepsilon_{15,yy}(t)$ of frame-II; (a) $|H_1(\omega)|$; (b) $\angle H_1(\omega)$; (c) $|H_2(\omega)|$; (d) $\angle H_2(\omega)$

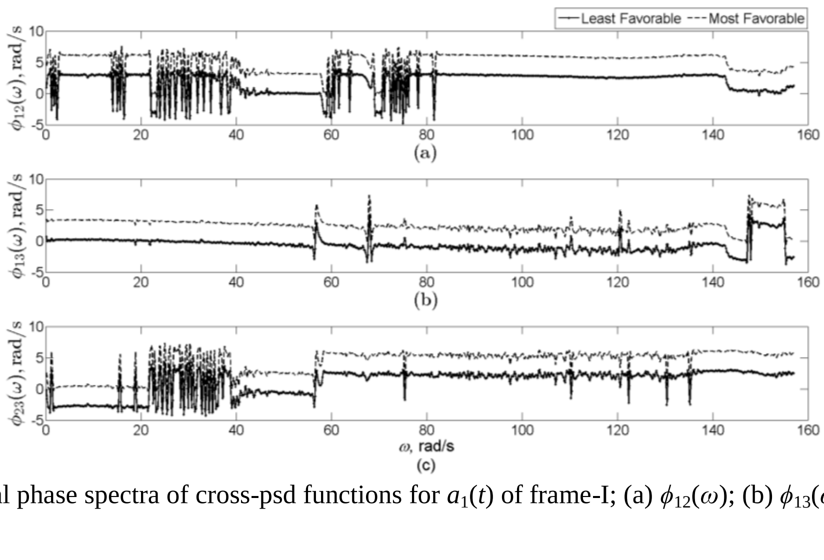

Fig. 5 Critical phase spectra of cross-psd functions for $a_1(t)$ of frame-I; (a) $\phi_{12}(\omega)$; (b) $\phi_{13}(\omega)$; (c) $\phi_{23}(\omega)$

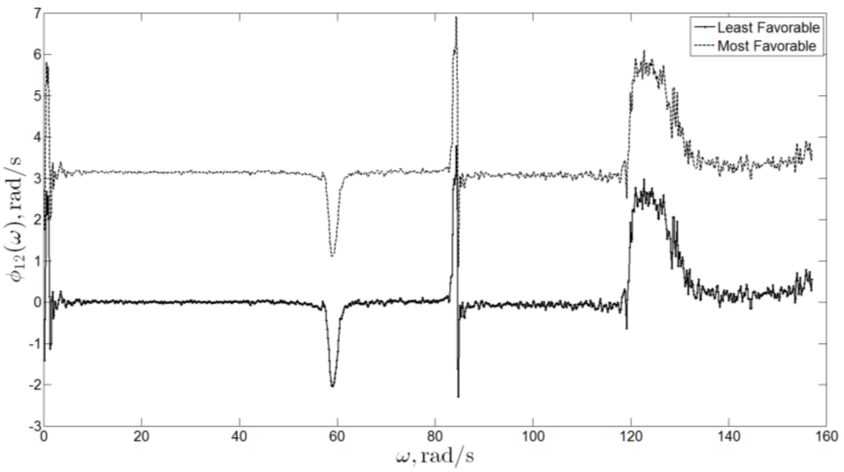

Fig. 6 Critical phase spectra $\phi_{12}(\omega)$ of cross-psd function for $\varepsilon_{15,yy}(t)$ of frame-II

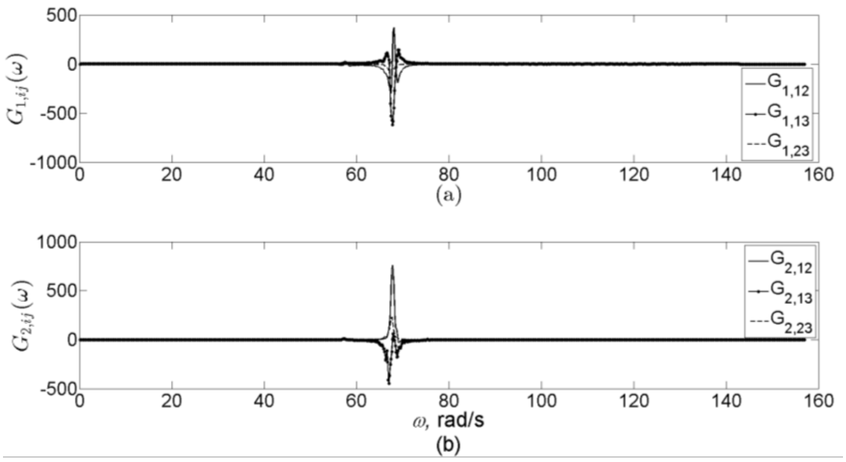

Fig. 7 $G_{1,ij}(\omega)$ and $G_{2,ij}(\omega)$ associated with $a_1(t)$ for frame-I; (a) $G_{1,ij}(\omega)$; (b) $G_{2,ij}(\omega)$; i,j=1,2,3 and i<j

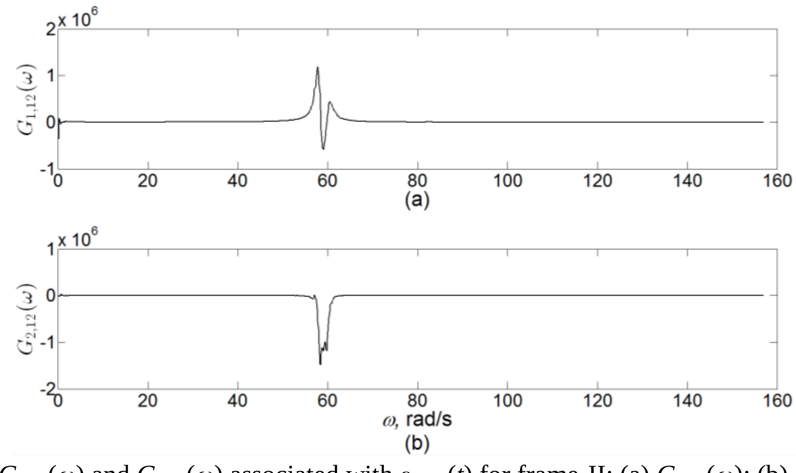

Fig. 8 $G_{1,12}(\omega)$ and $G_{2,12}(\omega)$ associated with $\varepsilon_{15,yy}(t)$ for frame-II; (a) $G_{1,12}(\omega)$; (b) $G_{2,12}(\omega)$

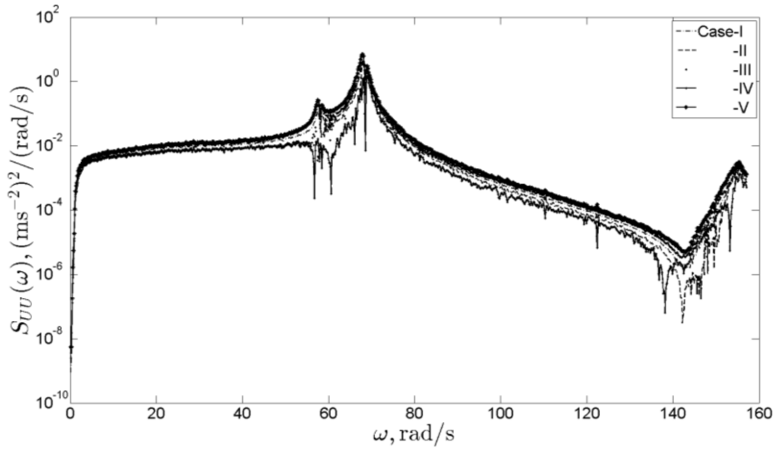

Fig. 9 Auto-psd function of acceleration $a_1(t)$ of frame-I for different load models

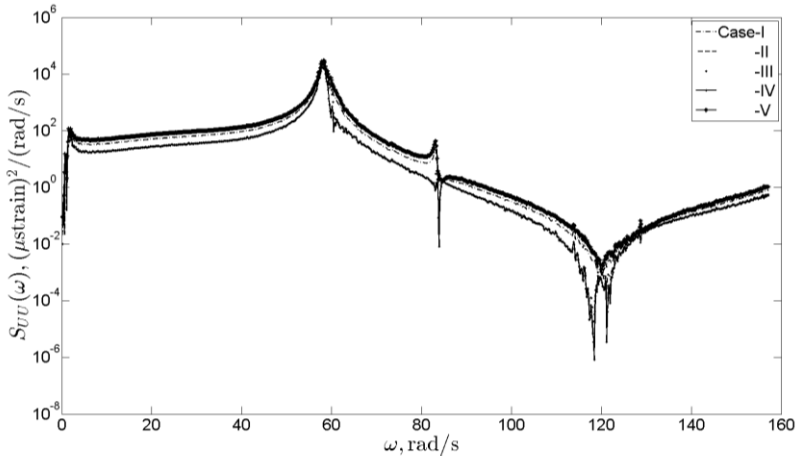

Fig. 10 Auto-psd function of strain $\varepsilon_{15,yy}(t)$ of frame-II for different load models

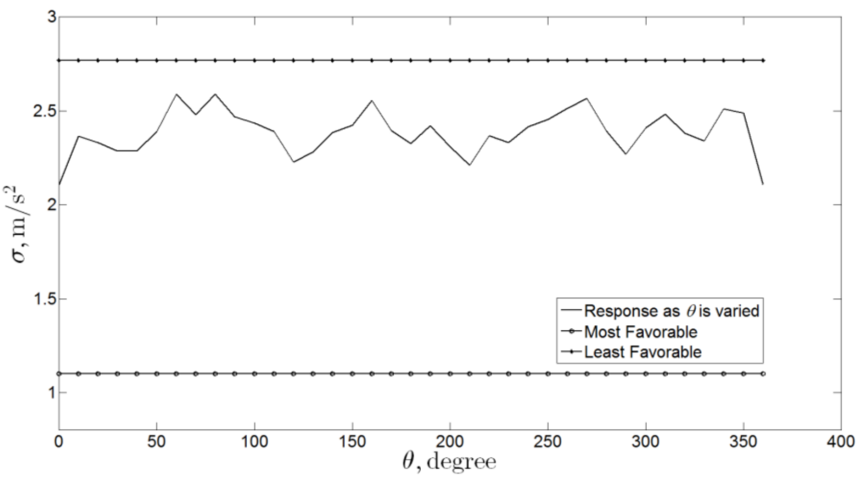

Fig. 11 Standard deviation of response $a_1(t)$ of frame-I as a function of angle of incidence θ

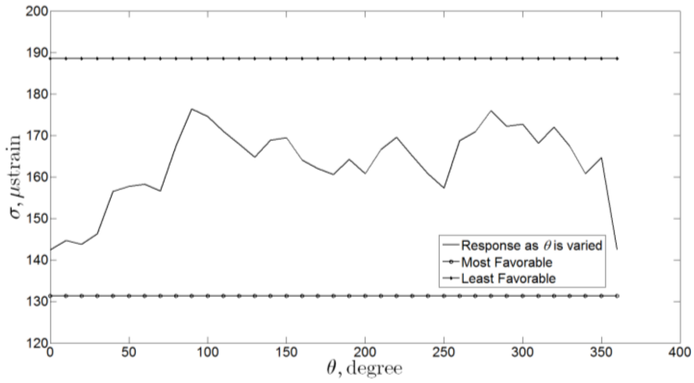

Fig. 12 Standard deviation of response $\varepsilon_{15,yy}(t)$ of frame-I as a function of angle of incidence θ

Table 1 Steady state standard deviations of accelerations and bending strains (in microstrains) for frame-I

S. No.	Response	Case-I	Case-II	Case-III	Case-IV	Case-V	Case-VI	Case-VII
1	a_1 (ms^{-2})	2.1078	1.9917	2.2179	1.1017	2.7699	2.1078	2.5906
2	a_2 (ms^{-2})	2.9277	2.9328	2.9225	2.0246	3.6116	2.6277	3.4943
3	a_3 (ms^{-2})	0.2913	0.3407	0.2356	0.2316	0.4745	0.2430	0.4755
4	α (rads^{-2})	3.7861	3.5513	4.0072	2.1554	4.9013	3.7861	4.7678
5	$\varepsilon_{1,yy}$	180.4577	174.4249	186.2952	91.2349	238.3403	144.1579	220.5909
7	$\varepsilon_{3,yy}$	114.2266	107.1109	120.9243	60.4332	149.8108	114.2266	140.0359
8	$\varepsilon_{4,xx}$	251.3623	248.3666	254.3228	159.4541	317.7111	251.3623	319.0065
9	$\varepsilon_{5,xx}$	200.8279	203.3359	198.2881	136.8029	248.8949	185.8279	242.8909
10	$\varepsilon_{6,yy}$	140.0583	130.7973	148.7437	72.9676	184.1422	140.0583	175.5264
11	$\varepsilon_{7,yy}$	261.7993	265.1871	258.3674	178.3418	324.4566	246.7993	321.0980

Table 2 Steady state standard deviations of accelerations and bending strains (in microstrains) for frame-II

S. No.	Response	Case-I	Case-II	Case-III	Case-IV	Case-V	Case-VI	Case-VII
1	$a_{1,x}$ (ms^{-2})	0.7916	0.7329	0.8462	0.6389	0.9192	0.7916	0.8849
2	$a_{2,x}$ (ms^{-2})	2.1415	2.1174	2.1655	1.8137	2.4255	2.1105	2.3864
3	$a_{2,y}$ (ms^{-2})	2.3262	2.3333	2.3191	2.1235	2.5126	2.1423	2.4995
4	$a_{3,x}$ (ms^{-2})	7.6484	7.3606	7.9257	6.6368	8.5410	7.0498	8.0772
5	$a_{3,y}$(ms^{-2})	7.9861	8.0239	7.9481	7.4814	8.4607	7.5931	8.3895
6	α_2 (rads^{-2})	3.3384	4.5831	1.1337	0.8352	4.6468	3.3384	4.0112
7	α_3 (rads^{-2})	4.4143	5.9935	1.7467	1.1363	6.1385	4.4143	5.3428
8	$\varepsilon_{1,yy}$	97.3820	102.4721	92.0108	66.8470	120.4077	95.6541	109.9644
9	$\varepsilon_{2,yy}$	173.1105	180.1826	165.7370	129.3393	207.8603	169.0044	193.9418
10	$\varepsilon_{4,xx}$	93.7609	80.6158	105.2771	70.1630	112.5137	93.2937	105.2744
11	$\varepsilon_{7,yy}$	74.5976	64.3493	83.5990	42.0211	96.7670	74.5976	83.6997
12	$\varepsilon_{8,yy}$	140.5639	139.3272	141.7898	110.1850	165.4560	140.1689	156.8956
13	$\varepsilon_{12,xx}$	144.0006	144.6620	143.3359	138.0682	149.6978	139.0002	149.8393
14	$\varepsilon_{15,yy}$	162.4670	176.7299	146.8253	131.3826	188.4933	142.4670	176.3676

5. Conclusions

The study develops an experimental procedure to determine optimal cross-psd function models for components of earthquake support motions which lead to bounds on response variance of a given structure. The cross-psd models are obtained in terms of a set of FRFs which can be measured experimentally and the bounds obtained on the response variance are mathematically the sharpest in nature. The development of these excitation and response models do not require idealized mathematical models to be made for structure being tested and, therefore, the proposed procedure is expected to be applicable in the study of complex systems, such as, machinery and equipment, which are not easy to model mathematically. Illustrations on two asymmetric frame models are presented which corroborate the inherent features of the proposed excitation and response models. The extension of these studies to investigate response of *active* system with moving elements (as in pumps, rotors, turbines, and computer CPU unit) is currently being pursued by the present authors. Likewise, questions on treating nonlinearities in the system characteristics and/or parametric action of vertical component of excitation while determining the input optimal cross-psd models experimentally are also being pursued.

References

Abbas, A.M. and Manohar, C.S. (2007), "Reliability-based vector nonstationary random critical earthquake excitations for parametrically excited systems", *Struct. Saf.*, **29**(1), 32-48.

Ammanagi, S. and Manohar, C.S. (2015), "Optimal cross-spectrum of road loads on vehicles: theory and experiments", *J. Vib. Control*, doi: 10.1177/1077546315570107.

Athanatopoulou, A.M. (2005), "Critical orientation of three correlated seismic components", *Eng. Struct.*, **27**(2), 301-312.

Bendat, J.S. (1998), *Nonlinear systems techniques and applications*, Wiley, New York.

Bendat, J.S. and Piersol, A.G. (2010), *Random Data: Analysis and Measurement Procedures*, Wiley-Blackwell, New York.

Clough, R.W. and Penzien, J. (1993), *Dynamics of Structures*, McGraw-Hill, New York.

Ewins, D.J. (2000), *Modal Testing, Theory, Practice, and Application*, Research Studies Press, Taunton.

Fujita, K., Yoshitomi, S., Tsuji, M. and Takewaki I., (2008), "Critical cross-correlation function of horizontal and vertical ground motions for uplift of rigid block", *Eng. Struct.*, **30** (5), 1199-1213.

González, J.V., Schroeder, M.O. and Martínez, J.D. (2015), "Combination rule for critical structural response in soft soil", *Eng. Struct*., **82**, 1-10.

IEEE-344 (2013), *IEEE Standards*, IEEE Recommended Practices for Seismic Qualification of Class 1E Equipment for Nuclear Power Generating Stations, New York.

Jaiswal, K. and Sinha, R. (2007), "Spatial variation of maximum considered and design basis earthquakes in peninsular India", *Curr. Sci.*, **92**(5), 639-645.

Kiureghian, A.D. and Nakamura, Y. (1993), "CQC modal combination rule for high-frequency modes", *Earthq. Eng. Struct. Dyn*., **22**(11), 943-956.

Kubo, T. and Penzien, J. (1979), "Analysis of three-dimensional strong ground motions along principal axes, San Fernando earthquake", *Earthq. Eng. Struct. Dyn*., **7**(3), 265-278.

Lopez, O.A. and Rorres, R. (1997), "The critical angle of seismic incidence and the maximum structural response", *Earthq. Eng. Struct. Dyn*., **26**(9), 881-894.

Lopez, O.A., Chopra, A.K. and Hernandez, J.J. (2000), "Critical response of structures to multicomponent earthquake excitation", *Earthq. Eng. Struct. Dyn.*, **29**(12), 1759-1778.

McConnel, K.G. (1995), *Vibration testing: Theory and Practice,* John Wiley, New York.

Menun, C. and Kiureghian, A.D. (1998), "A replacement for the 30%, 40%, and SRSS rules for multicomponent seismic analysis", *Earthq. Spectra*, **14** (1), 153-163.

Menun, C. and Kiureghian, A.D. (2000), "Envelopes for seismic response vectors. I: Theory", *J. Struct. Eng.*, **126**(4), 467-473.

Nigam, N.C. and Narayanan, S. (1994), *Applications of random vibrations*, Narosa publishers, New Delhi.

Papoulis, A. and Pillai, S.U. (2002), Probability, random variables and stochastic processes, Tata McGraw-Hill, New Delhi.

Reyes-Salazar, A., López-Barraza, A., López-López A. and Haldar, A. (2008), "Multi-component seismic response analysis - a critical review", *J. Earthq. Eng.*, **(12)**, 779-799.

Rezaeian, S. and Kiureghian, A.D. (2012), "Simulation of orthogonal horizontal ground motion components for specified earthquake and site characteristics", *Earthq. Eng. Struct. Dyn.*, **41**, 335-353.

Sarkar, A. and Manohar, C.S. (1996), "Critical cross power spectral density functions and the highest response of multi-supported structures subjected multi-component earthquake excitations", *Earthq. Eng. Struct. Dyn.*, **25**(3), 303-315.

Sarkar, A. and Manohar, C.S. (1998), "Critical seismic vector random excitations for multiply supported structures", *J. Sound Vib*., **212**(3), 525-546.

Takewaki, I. (2002), "Seismic critical excitation method for robust design: A review", *J. Struct. Eng.*, **128**(5), 665-672.

Takewaki, I. (2013), *Critical excitation methods in earthquake engineering*, Elsevier, New York, USA.

Torbol, M. and Shinozuka, M. (2012), "Effect of the angle of seismic incidence on the fragility curves of bridges", *Earthq. Eng. Struct. Dyn.*, **41**(14), 2111-2124.

Worden, K. and Tomlinson, G.R. (2001), *Nonlinearity in structural dynamics*, Institute of Physics Publishing, Bristol.

KT

Annexure A. Details of steel frame models studied

Figs. A1and A2 show the geometric details of the frames studied. Tables A1 and A2 summarize the location and sensors types used in the experimental study.

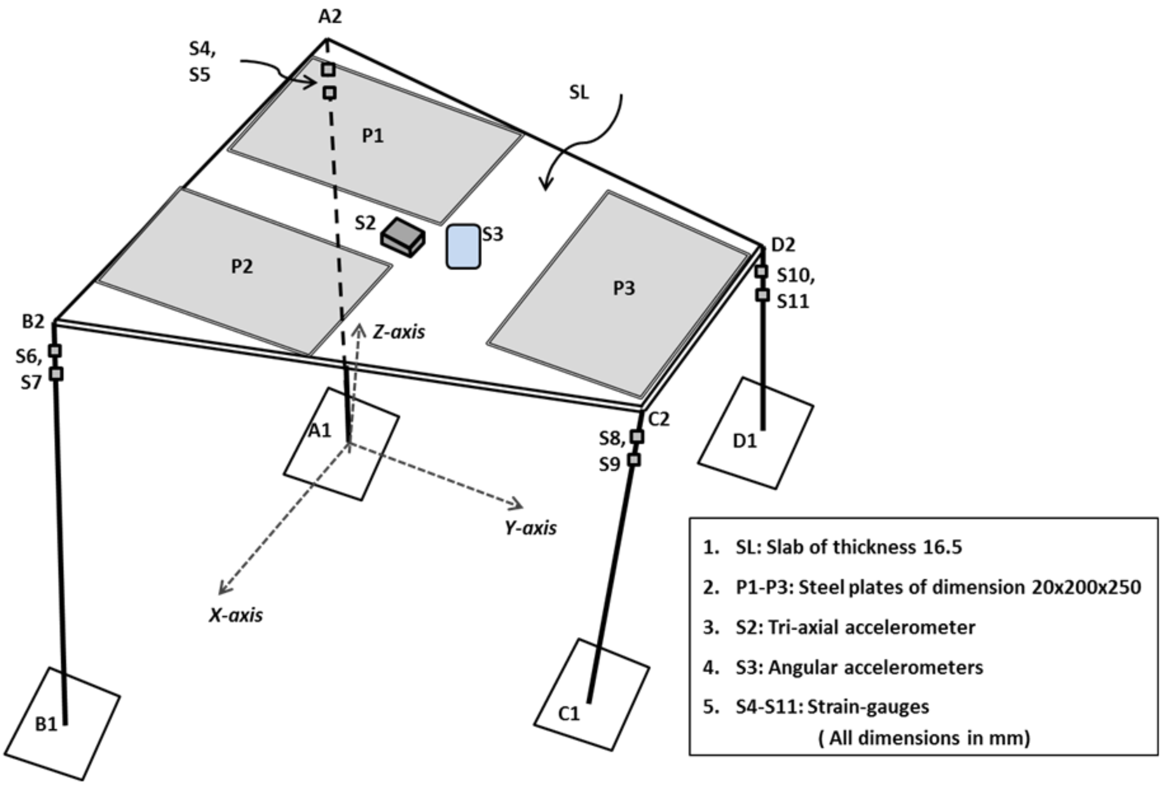

Fig. A1 Details of Frame-I

Table A1 Geometric details and locations of sensors used (Frame I)

Sl. No.	Point	Coordinates (in mm)			Sl. No.	Point	Coordinates (in mm)		
		X	Y	Z			X	Y	Z
1	A1	0	0	0	10	S3(α)	406.1	349.7	469.8
2	B1	770	0	0	11	S4($\varepsilon_{1,xx}$)	120.7	27.4	522.2
3	C1	725	578.5	0	12	S5($\varepsilon_{2,yy}$)	114.3	25.9	494.2
4	D1	8	578.5	0	13	S6($\varepsilon_{3,xx}$)	703.6	64.8	461.2
5	A2	129.3	29.3	559.5	14	S7($\varepsilon_{4,yy}$)	708	60.6	431.1
6	B2	697.8	70.5	501.3	15	S8($\varepsilon_{5,xx}$)	614.4	641.3	356
7	C2	602.2	648.2	395.5	16	S9($\varepsilon_{6,yy}$)	623.4	636	326.3
8	D2	196.5	593.7	434.4	17	S10($\varepsilon_{7,xx}$)	181.2	592.3	395.8
9	S2 (a_1,a_2 and a_3)	407.2	306.8	478.5	18	S11($\varepsilon_{8,yy}$)	178.4	591.3	366.8

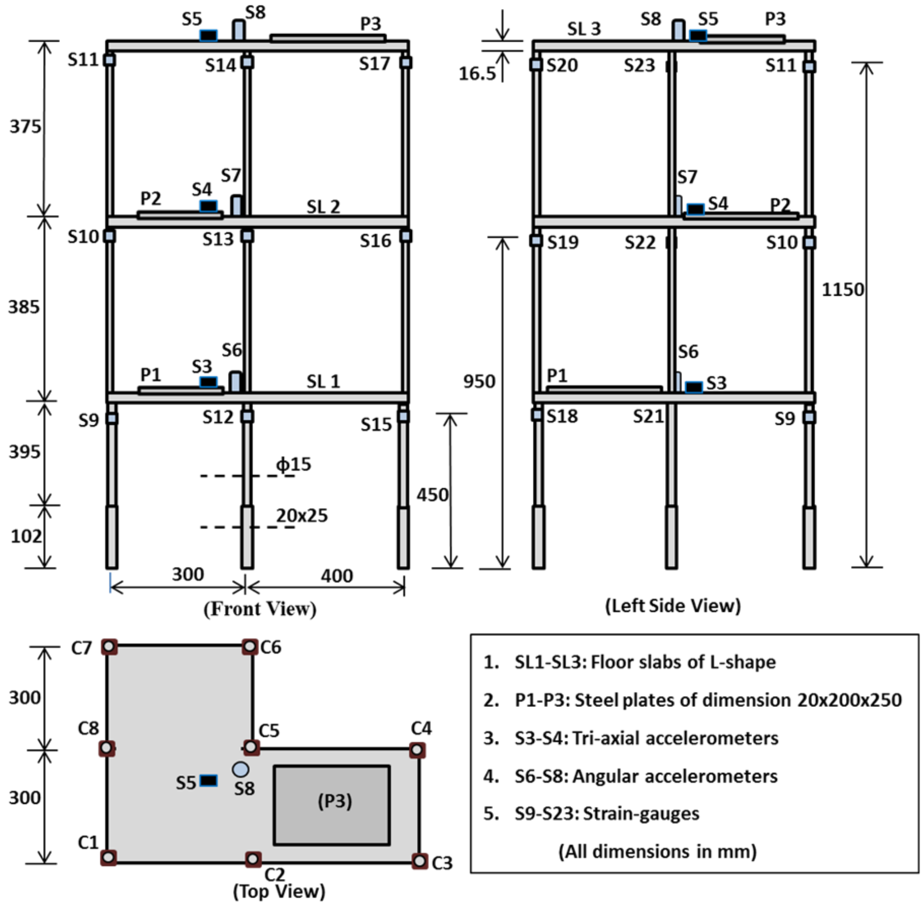

Fig. A2 Details of Frame-II

Table A2 Locations of sensors used (Frame II)

Sl. No.	Sensor	Response variable	Sl. No.	Sensor	Response variable
1	S1	a_{tx}	13	S13	$\varepsilon_{4,yy}$
2	S2	a_{ty}	14	S14	$\varepsilon_{13,yy}$
3	S3	$a_{1,x}$, $a_{1,y}$ and $a_{1,z}$	15	S15	$\varepsilon_{6,xx}$
4	S4	$a_{2,x}$, $a_{2,y}$ and $a_{2,z}$	16	S16	$\varepsilon_{5,xx}$
5	S5	$a_{3,x}$, $a_{3,y}$ and $a_{3,z}$	17	S17	$\varepsilon_{4,xx}$
6	S6	α_1	18	S18	$\varepsilon_{9,yy}$
7	S7	α_2	19	S19	$\varepsilon_{8,yy}$
8	S8	α_3	20	S20	$\varepsilon_{7,yy}$
9	S9	$\varepsilon_{3,yy}$	21	S21	$\varepsilon_{12,xx}$
10	S10	$\varepsilon_{2,yy}$	22	S22	$\varepsilon_{11,xx}$
11	S11	$\varepsilon_{1,yy}$	23	S23	$\varepsilon_{10,xx}$
12	S12	$\varepsilon_{15,yy}$			